ER-Rhythm: Coupling Exercise and Respiration Rhythm Using Lightweight COTS RFID

YANNI YANG*, The Hong Kong Polytechnic University, China
JIANNONG CAO, The Hong Kong Polytechnic University, China
XIULONG LIU, Tianjin University, China

The locomotor-respiratory coupling (LRC) ratio of a person doing exercise is an important parameter to reflect the exercise safety and effectiveness. Existing approaches that can measure LRC either rely on specialized and costly devices or use heavy sensors, bringing much inconvenience to people during exercise. To overcome these limitations, we propose ER-Rhythm using low-cost and lightweight RFID tags attached on the human body to simultaneously extract and couple the exercise and respiration rhythm for LRC estimation. ER-Rhythm captures exercise locomotion rhythm from the signals of the tags on limbs. However, extracting respiration rhythm from the signals of the tags on the chest during exercise is a challenging task because the minute respiration movement can be overwhelmed by the large torso movement. To address this challenge, we first leverage the unique characteristic of human respiratory mechanism to measure the chest movement while breathing, and then perform dedicated signal fusion of multiple tags interrogated by a pair of antennas to remove the torso movement effect. In addition, we take advantage of the multi-path effect of RF signals to reduce the number of needed antennas for respiration pattern extraction to save the system cost. To couple the exercise and respiration rhythm, we adopt a correlation-based approach to facilitate LRC estimation. The experimental results show that LRC can be estimated accurately up to 92% – 95% of the time.

CCS Concepts: • **Human-centered computing** → **Ubiquitous and mobile computing systems and tools**; *Mobile devices*; • **Networks** → Mobile networks.

Additional Key Words and Phrases: exercise and respiration rhythm, RFID, phase

ACM Reference Format:
Yanni Yang, Jiannong Cao, and Xiulong Liu. 2019. ER-Rhythm: Coupling Exercise and Respiration Rhythm Using Lightweight COTS RFID. *Proc. ACM Interact. Mob. Wearable Ubiquitous Technol.* 3, 4, Article 158 (December 2019), 24 pages. https://doi.org/10.1145/3369808

1 INTRODUCTION

1.1 Motivation

Nowadays, indoor fitness training has become a popular choice for people to do regular exercise. However, many people fail to achieve safe and effective exercise due to the lack of measurements for the body physiological

*This is the corresponding author.

Authors' addresses: Yanni Yang, The Hong Kong Polytechnic University, The Hong Kong Polytechnic University, Hung Hom, Kowloon, Hong Kong, China, 17901076r@connect.polyu.hk; Jiannong Cao, The Hong Kong Polytechnic University, The Hong Kong Polytechnic University, Hung Hom, Kowloon, Hong Kong, China, jiannong.cao@polyu.edu.hk; Xiulong Liu, Tianjin University, Tianjin University, Yaguan Rd. No. 135, Jinnan District, Tianjin, China, xiulongliudut@gmail.com.

2474-9567/2019/12-ART158 $15.00
https://doi.org/10.1145/3369808

signals, which could result in serious physical injuries or visceral organ damage [3]. Various parameters have been proposed to analyze the physical and physiological information during exercise. One key parameter is the locomotor-respiratory coupling (LRC) ratio, which characterizes the correlation between the exercise locomotion and respiration rhythm. Researchers have found that there exists the tight coordination between the limb movement and respiration for many rhythmic exercise activities, *e.g.*, running, cycling and pedaling [12, 34]. Keeping harmonic coordination between locomotion and respiration during exercise not only reduces energy consumption and prolongs the training period, but also promotes the maintenance of the cardiopulmonary functions [27].

Experimental evidence and practical experiences have given many suggestions on how to exercise with an accurate way of breathing. LRC ratio is an essential parameter, which is defined as the frequency and phase locking between locomotion and respiration [11]. By monitoring the LRC during exercise, people can adjust their respiratory rhythm to maintain the LRC ratio at a stable and proper level, so that they can boost exercise performance and prevent getting hurt. Therefore, our work targets on accurately estimating the LRC ratio for coupling the exercise and respiration rhythm.

1.2 Limitation of Prior Art

Existing works primarily focus on the following three categories: (1) Exercise-only monitoring systems using cameras [23], inertial sensors [19] or wireless signals (*e.g.*, WiFi [39] and RFID [14]) to detect and evaluate the exercise performance for various exercise activities. These works only target on extracting the locomotion pattern during exercise while failing to capture the respiration information; (2) Respiration-only monitoring systems using wearable sensors (*e.g.*, chest belt and nostril sensor) or wireless signals (*e.g.*, WiFi [25, 26] and radar [35]). The on-body sensors are quite intrusive to users. For instance, the specialized chest band [7] which is tightly bound on the chest could make people uncomfortable for free breathing and exercise, especially for women. Although wireless signals provide a contact-free approach to detect the respiration, they can accurately monitor the respiration state merely when the person is in the quasi-static state, *e.g.*, sleeping and sitting; (3) Exercise and respiration rhythm monitoring systems including the cardiopulmonary exercise testing (CPET) [10] and smartphone-based systems [16, 17, 20]. CPET is expensive which can cost over \$2, 000 for one user per test. Besides, people need to wear facemask and ECG electrodes on the body during exercise, bringing much inconvenience. Smartphone-based systems are cost-effective compared with CPET. However, people need to put a microphone close to the mouth and nose on the face, meanwhile wearing the smartphone on the arm. Furthermore, extra sensors are required if leg movement needs to be monitored which brings more load and discomfort during exercise. Compared with these limitations, we may raise a question: *can we simultaneously extract and couple the exercise and respiration rhythm in a lightweight way using low-cost commercial devices?*

1.3 Our Approach

In our work, we employ commercial RFID devices to measure the LRC ratio. RFID tags are lightweight, offering a way for non-intrusive sensing to release people from wearing bulky sensors during exercise. In addition, RFID tags are quite cheap ($\$0.1 - 0.2$ per tag). People can share the low-cost service based on the RFID infrastructure deployed for public use, *e.g.*, in the gym. RFID tags can be attached on different body parts, so that different movements can be detected and distinguished. Therefore, we propose ER-Rhythm, which can simultaneously measure and couple the exercise and respiration rhythm with accurate LRC estimation during exercise. The system can be deployed in the indoor environment, like in the gym coaching session.

In ER-Rhythm, RFID tags are attached on the limbs and chest to extract the exercise limb movement and respiration rhythm, respectively. As shown in Fig. 1, two RFID antennas are deployed in front of and behind the person. The front antenna transmits signals to the tags on the limbs and front chest. The back antenna

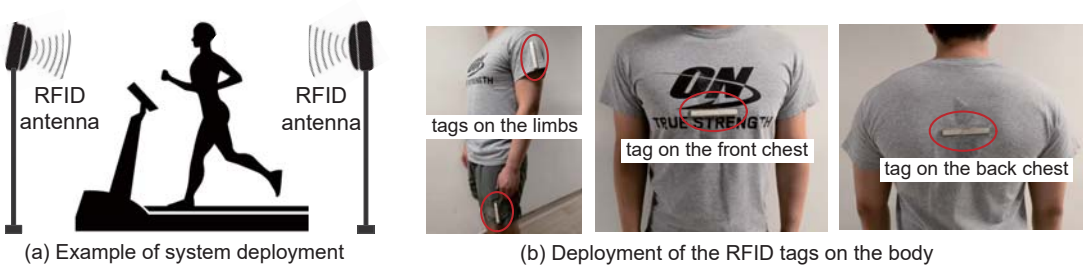

Fig. 1. Illustration of ER-Rhythm scenario and deployment of RFID tags.

interrogates the tag on the back chest. The backscattered signals reflected by all the tags are collected by the RFID reader for further processing. Our key observation is that the movements of different body parts during exercise affect the phase values of the RFID signals in distinct ways. The backscattered signals reflected by the tags on the limbs involve the limb movement pattern, which is called *limb movement effect*. For the tags attached on the chest, the backscattered signals involve the tiny chest movement caused by respiration (*respiration effect*) as well as the relatively large torso movement caused by the exercise locomotion (*torso movement effect*). The *torso movement effect* can be further divided, including the *random effect* due to the randomly unbalanced body trembling and the *periodic effect* generated by the cyclic exercise movements. In our work, we first study the feasibility to measure both the exercise limb movement and respiration rhythm by modeling the effects of different body movements on the phase values of RFID signals. Then, we estimate the exercise limb movement rate with the limb tags. The tiny respiration pattern is extracted after removing the effects from the large torso movement by synthesizing the information of multiple tags on the body. Finally, the patterns measured from the limb movement and respiration are coupled to estimate the LRC ratio. To further reduce the system cost, we make use of the multi-path effect of the backscattered signals to extract the exercise and respiration rhythm with only one antenna, which still achieves high LRC estimation accuracy.

1.4 Challenges

To simultaneously extract and couple the exercise and respiration rhythm while achieving accurate LRC estimation, however, is not a trivial task. The first challenge is to extract the chest movement pattern during respiration from the RFID signals. The chest movement displacement caused by respiration is tiny, making the phase changes of the signals to be quite small. We enhance the chest movement pattern by leveraging the unique characteristic of human respiratory mechanism that the front and back chest will expand and contract synchronously while breathing. By fusing both the front and back chest movement, a larger respiration pattern can be obtained.

Even if the chest movement pattern while breathing is enlarged, it is still too small to be distinguished from the large torso movement. Thereby, the second challenge is to eliminate the *torso movement effect*, especially for the *random effect* which is mixed with the respiration pattern in the chest tag signals. The *random effect* comes from the unbalanced torso trembling, whose pattern is unpredictable and untraceable. To solve this problem, we decompose the random torso movement along two dimensions and remove it based on the relative moving distances and directions of the two chest tags towards two antennas.

The third challenge is to accurately estimate the LRC ratio. Since the limb movement rate (f_l) is higher than the respiration rate (f_r), the torso *periodic effect* can be removed by applying the low-pass filter with f_l as the cutoff frequency. However, when f_l and f_r are close to each other, the *periodic effect* will leave residual effect on the respiration pattern due to the transition band of the low-pass filter. Besides, the estimation of f_r suffers from the low resolution when performing Fast Fourier Transformation (FFT) on the respiration signals with

limited length. Thus, LRC can be wrongly estimated with inaccurate f_r. To address the problem, we get inspired by the LRC theory that there are a set of LRC ratios for human-beings during exercise. So, we generate simulated respiration signals based on the known LRC ratios and f_l. Then, a cross-correlation array is calculated between the real respiration signals and each of the simulated signals. The final LRC is decided as the one with the highest correlation value.

1.5 Contributions

In this paper, we make the following three contributions: (1) We propose ER-Rhythm, which is the first work that uses COTS RFID to extract respiration pattern during exercise and couples the exercise and respiration rhythm in a lightweight and low-cost way. (2) We perform in-depth analysis about the effects of the exercise movements and respiration on the RFID signals. The tiny *respiration effect* is fully extracted against the large *torso movement effect*. Meanwhile, we employ the multi-path effect to reduce needed antennas. Finally, we adopt a correlation-based approach to couple the exercise and respiration rhythm for LRC estimation. (3) The ER-Rhythm is implemented to evaluate the LRC estimation performance with different kinds of exercise activities under different settings in the real environment. Extensive experiments show that our system can estimate the LRC ratio accurately up to $92\% - 95\%$ of the time.

The rest of the paper is organized as follows. Section 2 introduces the basics of LRC and analyzes the effects of limb movement and respiration on the RFID phase values. In Section 3, we illustrate the overview of the ER-Rhythm and the detailed design of each module in the system. Section 4 presents our experimental setup and results on LRC estimation under different scenarios. The related work is given in Section 5. At last, we discuss the future work in Section 6 and make the conclusion in Section 7.

2 UNDERSTANDING THE EXERCISE AND RESPIRATION RHYTHM

In this section, the preliminary knowledge of the locomotor-respiratory coupling is introduced first. Then, we perform analysis on using the RFID signals for extracting the exercise and respiration rhythm.

2.1 Locomotor-Respiratory Coupling

LRC is defined as the frequency and phase locking between the locomotor and respiratory systems [22]. According to the LRC theory [13], for humans doing exercise, there are a set of coupling ratios as listed in Table 1, denoted as LRC list. Taking the LRC of $3:1$ for the cycling activity as an example, it means the person breathes 1 time with 3 rounds of periodic limb movement. There are integer LRC ratios, *i.e.*, $5:1$, $4:1$, $3:1$, $2:1$, $1:1$, and non-integer LRC ratios, *i.e.*, $5:2$, $5:3$, $3:2$, $4:3$, in the LRC list. Researchers have given evidence in [12, 34] that integer LRC ratios appear more frequently than non-integer ratios. For most exercisers, there are dominant LRC (DC) and secondary LRC (SC) [31]. DC is the main LRC for most of the exercise duration. While SC, which is usually the closest LRC near DC, will appear for the purpose of adjusting the exercise rhythm gradually when the exerciser changes the locomotory speed. SC can reflect how the exerciser responds to the change of exercise intensity by adjusting the respiration. The type of exercise activity is one of the modulators of the LRC. For example, LRC ratios in running are typically $2:1$, $3:1$, and $4:1$, among which $2:1$ is the commonest ratio. For cycling, common LRC ratios are $2:1$ and $3:1$, while $1:1$ is more frequently present in weightlifting. The personal trainers usually advise people to breathe within the common range of LRC for the specific activity. Exercisers

Table 1. Common LRC ratios for human-beings during exercise

LRC ratio	5:1	4:1	3:1	5:2	2:1	5:3	3:2	4:3	1:1

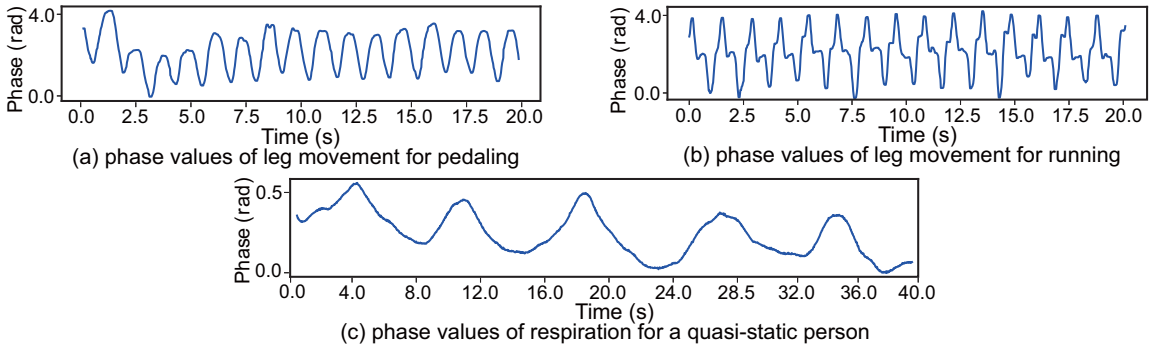

Fig. 2. Phase series of limb movements for exercise activities and chest movement for respiration

with higher LRC may overload themselves without sufficient oxygen supply. While lower LRC indicates that exercisers may achieve less effective exercise training.

The way to measure LRC, which has been adopted by many researchers, is to divide the locomotion movement rate by the respiration rate during a period and approximate the result to its nearest ratio in the LRC list [28]. There can be few cases, *e.g.*, when the real LRC is $11:4$, while the determined LRC is $3:1$. However, according to the studies in sports training [34] and interview replies from personal trainers, it is sufficient to provide the common LRC ratios in the LRC list to exercisers for training guidance. Therefore, the result when we measure LRC is one of the values in the LRC list.

We select some in-place and rhythmic activities to measure the LRC considering two aspects. First, the selected activities should cover different types of exercise to test whether the system can work for different activities. Second, since the torso movement brings more noises for respiration pattern extraction, there should be exercise activities that involve different magnitudes of torso movement to evaluate our approach. Therefore, we choose both aerobics (running, rowing, pedaling, and cycling) and anaerobic activity (weightlifting). For the scale of torso movement, large torso movement appear during running and rowing, while pedaling, cycling and weightlifting involve less torso movement. The intensity for the activities is controlled by the exerciser with different speeds or frequencies.

2.2 RFID Phase Values for Exercise or Respiration Movements

To monitor the exercise and respiration activity, the phase value of RFID signals is used. The phase value is a basic metric which reveals the relative distance information between the signal transmitter and receiver. For the RFID signals, the distance d between the antenna and the tag can influence the phase value θ, which can be represented as follows.

$$\theta = \left\{ \frac{2d}{\lambda} \cdot 2\pi + \epsilon \right\} \mod 2\pi \tag{1}$$

λ is the wavelength ($\approx 32.4\ cm$ here), and ϵ is the phase shift with a fixed value caused by the hardware imperfection and environmental effects. Since we focus on the change of the phase values during body movements, the existence of ϵ will not affect the result. When the tag is attached on the body, it will move along with the body during exercise, and the phase values will change accordingly. The limb movement can bring around $5\ cm - 15\ cm$ change on d depending on the position of the tag on the limb. While the chest movement during respiration only incurs about $5\ mm - 10\ mm$ change on d [32], so the phase changes incurred by the respiration would be quite small.

The phase values of the tags on the limbs are shown in Fig. 2(a)-(b) for the pedaling and running activities as examples. They show clear and periodic patterns of limb movements. Then, a person is asked to breathe normally

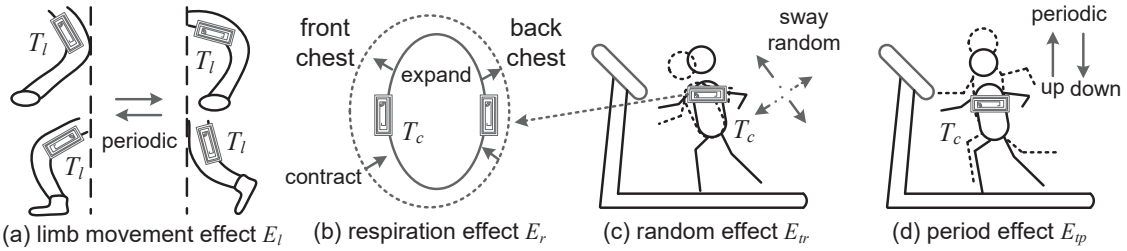

Fig. 3. Illustration of different movement effects on the tags for the running activity

in a quasi-static standing state, and the phase values of the tag on the front chest are shown in Fig. 2(c), in which 5 times of sinusoidal breathing cycles are present. The phase value for respiration is much smaller than the limb movement. Furthermore, the respiration signals of the chest tag during exercise would suffer from more noises due to the effects of the large torso movement.

2.3 Modeling the Respiration Activity during Exercise

In this subsection, we analyze the effects of the limb movement and respiration on the RFID signals. The tags on the limbs, *i.e.*, the leg and arm, are denoted as T_l, and the tags on the chest are represented as T_c. For T_l, it is mainly affected by the *limb movement effect* (E_l), which is the cyclic movement of arm and leg, as shown in Fig. 3(a). The phase value θ_l of T_l can be expressed as below.

$$\theta_l = \left\{ \frac{2(d_l + d_{E_l})}{\lambda} \cdot 2\pi \right\} \mod 2\pi,\ d_{E_l} = A_1 \sin(2\pi f_l + \phi_1) \tag{2}$$

d_l is the initial distance between the tag and the antenna. d_{E_l} characterizes the periodic limb movement into a sinusoidal signal, with f_l as the limb movement rate and ϕ_1 as the initial phase.

For T_c, it is directly influenced by two sources of movement effects via the line-of-sight (LOS) path, as shown in Fig. 3(b)-(d), one is the target *respiration effect* (E_r) caused by the chest movement for observing the respiration pattern during exercise (Fig. 3(b)), the other is the *torso movement effect* (E_t). The *torso movement effect* can be further divided into two parts: *random effect* (E_{tr}) and *periodic effect* (E_{tp}). The *random effect* is caused by the random movement during exercise. Although most indoor exercise activities are in-place movements, the torso could move randomly to the right or the left, forward or backward (Fig. 3(c)), as the body cannot keep definitely balanced while exercising. The *periodic effect* is the product of the cyclic torso movement during exercise. For example, the person's torso would sway up and down while running on a treadmill (Fig. 3(d)). As a result, the *periodic effect* could synchronize with the *limb movement effect*. The *torso movement effect* could degrade the respiration pattern in the phase values. This is because that the torso movement is larger than the minute respiration movement. Thus, the respiration pattern can be overwhelmed by the presence of torso movement. There are also indirect and minor multi-path effects brought by the limb movement on T_c, denoted as $d_{E_{lm}}$, which is consistent with the *limb movement effect*. Thus, the phase values θ_c of T_c can be represented as follows.

$$\begin{gathered} \theta_c = \left\{ \frac{2(d_c + d_{E_r} + d_{E_t} + d_{E_{lm}})}{\lambda} \cdot 2\pi \right\} \mod 2\pi,\ d_{E_r} = A_2 \sin(2\pi f_r + \phi_2) \\ d_{E_t} = d_{E_{tr}} + d_{E_{tp}},\ d_{E_{tp}} = A_3 \sin(2\pi f_l + \phi_3),\ d_{E_{lm}} = A_4 \sin(2\pi f_l + \phi_4),\ A_4 < A_3 \end{gathered} \tag{3}$$

The respiration effect d_{E_r} is also converted into a sinusoidal signal, with f_r as the respiration rate.

To extract the exercise locomotion pattern, we can leverage the phase values of T_l and estimate the limb movement rate f_l via peak detection. However, the large *torso movement effect*, mixed with *respiration effect*,

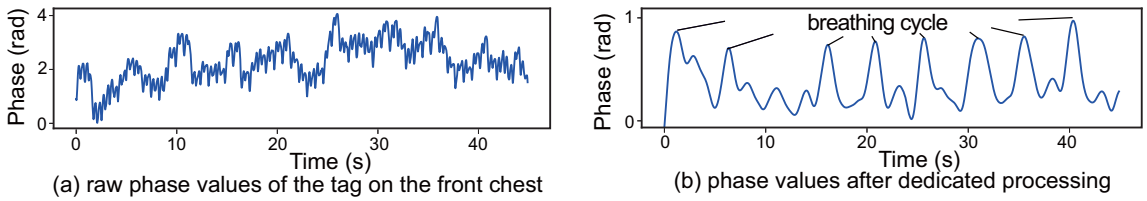

Fig. 4. Respiration pattern of the tag on the front chest and that of after our processing.

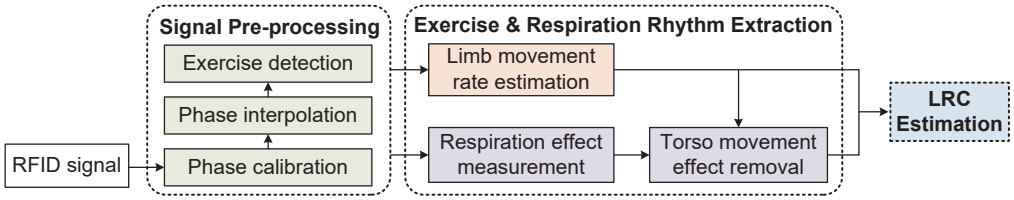

Fig. 5. The ER-Rhythm system overview.

should be removed from the signals of T_c to recover the clear respiration pattern. Fig. 4(a) depicts the raw RFID phase values of the tag on the front chest during pedaling, which are quite messy to see the periodic respiration pattern due to the existence of the *torso movement effect*. The large wave changes in the signals are brought by the *random effect*, and the small the frequent fluctuations are caused by the *periodic effect*. Fig. 4(b) shows the recovered respiration signals with clear and periodic respiration cycles after our dedicated processing, which will be introduced in the next section.

3 ER-RHYTHM SYSTEM DESIGN

In this section, we will articulate the system workflow with a detailed introduction of each module.

3.1 System Overview

The sketch of the ER-Rhythm system is shown in Fig. 5. It consists of three phases: Signal Pre-processing, Exercise and Respiration Rhythm Extraction, and LRC Estimation. The inputs are the raw RFID signal measurements, including the antenna ID, tag ID, time and phase values. First, the raw phase values of all the tags are denoised via phase calibration, smoothing, and interpolation. Then, the phase series for the exercise activity are detected and segmented into small windows with a fixed length. Next, the phase series collected from T_l and T_c are used to extract the exercise limb movement and respiration pattern. The limb movement rate is calculated from the phase values of the tags on the limb. Meanwhile, the respiration rhythm is obtained through *respiration effect* measurement and removal of the *torso movement effect* on the respiration signals. Based on the chest movement mechanism during breathing, we investigate the usage of two tags on the front and back chest to enlarge the respiration pattern. Finally, the exercise and respiration rhythm is coupled to estimate the LRC ratio. Instead of calculating the LRC ratio by directly dividing the respiration rate over the limb movement rate, the LRC ratio is estimated using a correlation-based approach, which maps the coupling of the limb movement and respiration by generating template respiration signals based on the set of potential LRC ratios.

3.2 Signal Pre-processing

The raw phase values are first calibrated to remove the half-wave effect and unwrapped. Since the tags respond in a randomly selected slot to the signals transmitted from the antenna, the sampling rates and timestamps for

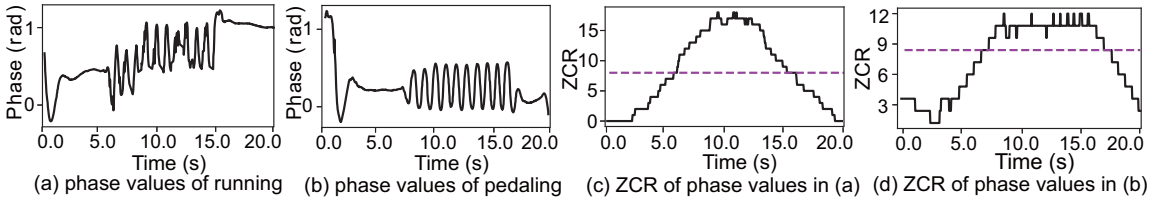

Fig. 6. Exercise detection by calculating the ZCR of the phase values

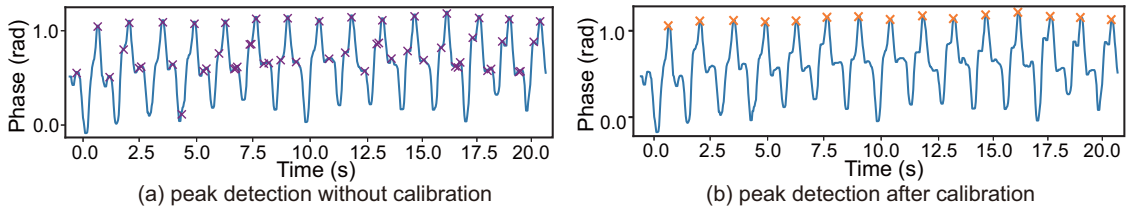

Fig. 7. Limb movement rate extraction with peak detection

different tags are not the same. Therefore, the phase series of all the tags are interpolated with the same sampling rate, which is 50 Hz. For the tags on the limb, the median filter is applied to smooth the phase values. Next, we detect the exercise activity during which the LRC estimation is performed. We observe the phase values of T_l with and without exercise movements in Fig. 6(a)-(b). The first and the last parts are the start and end of the exercise. The sinusoidal wave in the middle is caused by the periodic limb movements. For each time window, we remove the mean of the phase values to create a waveform oscillating around 0. It can be seen that, for the periodic movements, the phase values go cross the zero line more frequently than those of the start and end period. Therefore, we use a sliding window to divide the phase series and the zero-crossing rate (ZCR) is calculated for each sliding window. Then, a threshold is selected to detect the exercise movements. The ZCR values are illustrated in Fig. 6(c)-(d). Here, as the human respiration rate is $10 - 30$ breath per minute, the sliding window is 5s-wide so that it involves at least one breathing cycle. The interval of the sliding window is 2 samples. The threshold is decided by the limb movement rate for the exercise activity. For example, the number of cycles during running and pedaling is normally above 40 per minute [5, 6]. So, the threshold for the ZCR is calculated as 8 (40/60*6*2). The horizontal dash line in Fig. 6(c)-(d) is the threshold. The windows whose ZCRs are above the threshold will be collected. Then, the phase time series of all the tags during the exercise activity are segmented into fix-length time windows, *i.e.*, 20 s.

3.3 Limb Movement Rate Estimation

The limb movement rate f_l is estimated from the signals of the tag on the limb. For running, cycling and pedaling, f_l is estimated with the tag on the leg. For weightlifting and rowing, f_l is obtained with the tag on the arm. The limb movement pattern in Fig. 2(a)-(b) presents sinusoidal wave which inspires us to detect the limb movement cycle via peak detection. However, since the peak detection algorithm identifies the peak whose neighbor value is smaller than it, there are many fake peaks in the phase series as shown in Fig. 7(a). To remove the fake peaks that do not correspond to the real movement cycle, we set a threshold for the distance between two neighbor peaks. For runnin, the stride frequency is usually in the range of [90, 120] cycles per minute [5]. For cycling and pedaling, the number of revolutions is within 80 rounds per minute [6]. For rowing and weightlifting, the number of cycles could be less, which is below 40 times per minute. Therefore, we can calculate the minimum interval σ_t between two movement cycles and discard the peaks that are too close to each other. In addition, we only

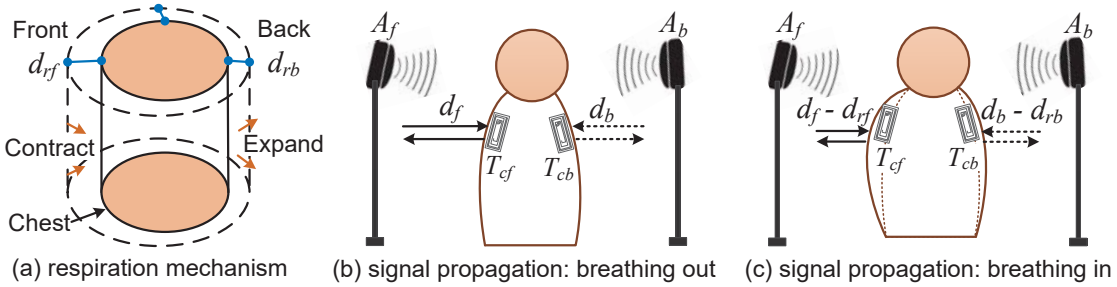

(a) respiration mechanism (b) signal propagation: breathing out (c) signal propagation: breathing in

Fig. 8. Chest movement modeling during respiration and the propagation of the RFID signals

keep the peaks whose height are higher than the mean value σ_m of the phase series. In Fig. 7(b), the peaks that represent the breathing cycles are detected. Then, the number of peaks is counted in a time window t as p_n. Since f_l is relatively stable within a short period of time, the limb movement rate f_l is estimated by $f_l = p_n/t$.

3.4 Respiration Pattern Extraction

Next, we will extract the respiration pattern involved in the phase values of T_c via respiration effect measurement and torso movement effect removal.

3.4.1 Respiration Effect Measurement. We employ the respiration mechanism, as shown in Fig. 8(a), to fully investigate the effects of chest displacement on the RFID phase values. When a person breathes in and out, the whole chest, which is simplified into a cylinder, will expand and contract accordingly [38]. In this process, there would be displacement change in the front, mediolateral and back dimension of the chest. During exercise, the mediolateral dimension change could be buried by the arm movement. But the front and back dimension can be fused together to extract the respiration effect, instead of only exploiting the front dimension change. In this way, the respiration pattern can be more obvious. Therefore, we attach one tag on the front chest and one tag on the back chest. Then, two antennas are put right in front of and behind the target person to interrogate the front tag and back tag, respectively, as shown in Fig. 8(b)-(c). Suppose that the respiration can lead to d_{rf} and d_{rb} displacement change of the front chest and back chest, respectively. d_{rf} is commonly larger than d_{rb}.

For the tag on the front chest (T_{cf}), the initial distance between T_{cf} and the front antenna (A_f) is d_f. When breathing in, the front chest will expand and move towards A_f, making the phase values of T_{cf} decrease. When breathing out, the chest will contract which leads to the increase of the phase values of T_{cf}. Then the phase difference $\Delta\theta_f$ of T_{cf} between breathing in ($(\theta_f)_{in}$) and breathing out ($(\theta_f)_{out}$) is:

$$\Delta\theta_f = \left|(\theta_f)_{in} - (\theta_f)_{out}\right| = \left|\left(\frac{2d_f - 2d_{rf}}{\lambda} - \frac{2d_f}{\lambda}\right)\cdot 2\pi\right| \mod 2\pi = \left\{\frac{2d_{rf}}{\lambda}\cdot 2\pi\right\} \mod 2\pi. \tag{4}$$

For the tag on the back chest (T_{cb}), the initial distance between T_{cb} and the back antenna (A_b) is d_b. When breathing in, the signal's traveling distance will drop by $2d_{rb}$ with the back chest expanding and moving backward. While for breathing out, the signal traveling distance will increase by $2d_{rb}$ with the back chest contracting and moving forward. If we add the phase values of T_{cf} and T_{cb}, the sum values while breathing in and out can be represented as below.

$$(\theta_f + \theta_b)_{in} = \left\{\frac{2(d_f - d_{rf}) + 2(d_b - d_{rb})}{\lambda}\cdot 2\pi\right\} \mod 2\pi \tag{5}$$

$$(\theta_f + \theta_b)_{out} = \left\{\frac{2d_f + 2d_b}{\lambda}\cdot 2\pi\right\} \mod 2\pi \tag{6}$$

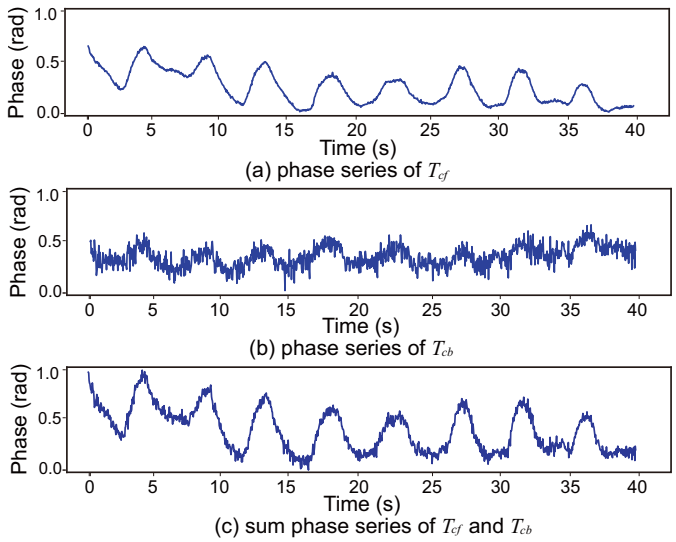

Fig. 9. Respiration phase series of T_{cf}, T_{cb} and their sum

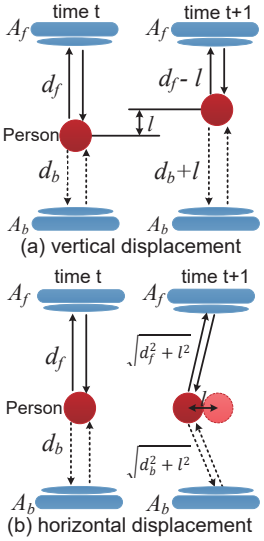

Fig. 10. Torso random effect modeling

Accordingly, the phase difference $\Delta(\theta_f + \theta_b)$ between breathing in and breathing out can be expressed as:

$$\Delta(\theta_f + \theta_b) = \left|(\theta_f + \theta_b)_{in} - (\theta_f + \theta_b)_{out}\right| = \left\{\frac{2(d_{rf} + d_{rb})}{\lambda} \cdot 2\pi\right\} \mod 2\pi. \tag{7}$$

Comparing Equ. (4) with Equ. (7), the phase difference of the summation of T_{cf} and T_{cb} is $2d_{rb}/\lambda$ larger than that of the single T_{cf}. In this way, the respiration pattern can be amplified. To verify it, we make one person to breathe in the quasi-static state, and measure the phase values of T_{cf}, T_{cb} and calculate the sum of T_{cf} and T_{cb}, as depicted in Fig. 9. It shows that the phase series of T_{cf} and T_{cb} are in-phase with each other. The peaks and valleys in the phase series when breathing out and breathing in are generally synchronized. It also shows that the magnitude of the phase values of T_{cb} is smaller than that of T_{cf}, since $d_{rb} < d_{rf}$. Most importantly, the summation of T_{cf} and T_{cb} shows larger amplitude for the respiration pattern in Fig. 9(c). Therefore, the phases values of T_{cf} and T_{cb} are added together for measuring the respiration chest movement.

3.4.2 Torso Movement Effect Removal. In subsection 2.3, we mention the *torso movement effect*, including the *random effect* and *period effect*, can overwhelm the respiration signals for the tags on the chest. Thus, we need to eliminate the effects caused by the torso movement to capture clear respiration pattern.

For the *random effect*, we divide the random torso movements into two parts. One is the vertical displacement (move forward and backward) and the other is horizontal displacement (move to the left and right). First, we show how the vertical displacement affects the phase values. As illustrated in Fig. 10(a), the torso moves l forward to A_f. Then the phase values of T_{cf} will decrease $\frac{2l}{\lambda}$. Suppose l is 5 cm, as the in-place exercise usually results in tiny torso swaying movement. Compared with the displacement of the chest while breathing, which is in the range of [5 mm, 10 mm] for the front chest [32], the vertical displacement l could bring large effect on the phase values. For T_{cb}, the phase values will increase inversely. Next, we discuss the effects of the horizontal displacement. As depicted in Fig. 10(b), the person moves to the left with distance of $l = 5$ cm. Suppose the distance between T_{cf} and A_f is $d_f = 1$ m, then the phase values will increase $\frac{2(\sqrt{d_f^2+l^2}-d_f)}{\lambda}$. The $(\sqrt{d_f^2 + l^2} - d_f)$ is only around 1 mm, which is quite small compared with the effects of vertical displacement $l = 5$ cm, so that the horizontal

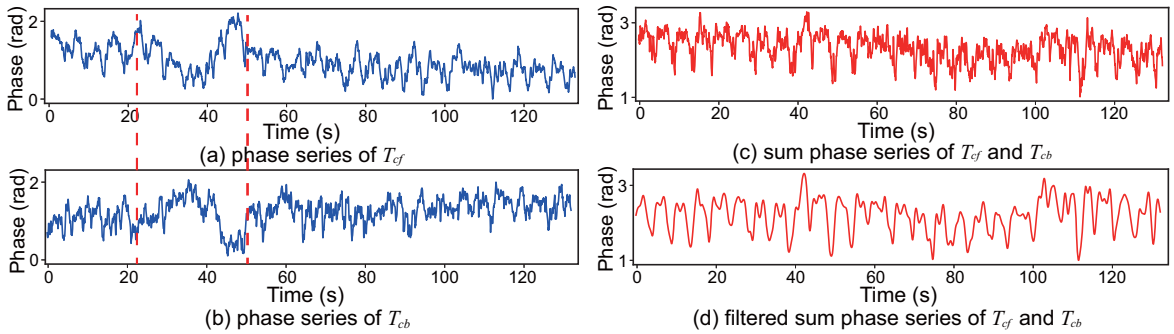

Fig. 11. Respiration phase series with effect from torso movements and removal of torso movement effect

displacement can be ignored. Therefore, we only need to consider the effects of the vertical displacement. We find that the vertical displacement brings opposite effects on the T_{cf} and T_{cb}. More specifically, if the person does not move, the summation of the phase values of T_{cf} and T_{cb} can be represented as below.

$$\theta_f + \theta_b = \left\{ \frac{2(d_f + d_b)}{\lambda} \cdot 2\pi \right\} \mod 2\pi \tag{8}$$

If the person's torso moves forward l, the propagation path of T_{cf} will drop from $2d_f$ to $2d_f - 2l$, while the path of T_{cb} will increase from $2d_b$ to $2d_b + 2l$. Then, the phase summation of T_{cf} and T_{cb} is as follows.

$$\theta_f + \theta_b = \left\{ \frac{2(d_f - l)}{\lambda} \cdot 2\pi + \frac{2(d_b + l)}{\lambda} \cdot 2\pi \right\} \mod 2\pi = \left\{ \frac{2(d_f + d_b)}{\lambda} \cdot 2\pi \right\} \mod 2\pi \tag{9}$$

Thereby, the distance l is removed in Equ. (9) by using the summation of the T_{cf} and T_{cb}. Here, we show the phase series for T_{cf} and T_{cb} when the person moves forward and backward towards the A_f while running in Fig. 11(a) and Fig. 11(b), respectively. They show that the phase values between the two vertical dashed lines experience a large change. For T_{cf}, the phase values first decrease and then increase, while T_{cb} shows the opposite trend. The summation phase series are shown in Fig. 11(c), in which the large phase changes caused by the random torso movement are offset. In this way, the random effect is eliminated and we can obtain relatively clear respiration pattern.

For the *period effect* which synchronizes with the limb movement, it incurs small and high-frequency fluctuations in the phase values, as shown in Fig. 11(c). Considering that the limb movement rate is generally higher than the respiration rate during exercise, we apply a third-order Butterworth low-pass filter with f_l as the cutoff frequency to remove the *period effect*. The phase series after the low-pass filter is depicted in Fig. 11(d), which shows the periodic pattern of the respiration rhythm.

3.4.3 Reduce the Usage of Two Antennas to One. To extract the clear respiration pattern from the RFID signals, multiple RFID tags and two antennas are employed. The usage of the front antenna A_f is to measure the signals of T_l and T_{cf}, and the back antenna A_b will interrogate T_{cb}. Although the RFID antenna does not cost much for the deployment of the system, it could be more cost-effective if we can reduce two antennas to one with similar results on respiration pattern extraction. In this way, we not only save the cost but also save the space for monitoring. From this point of view, we exploit the multi-path effects of the RF signals so that only A_f is required to measure the signals of all the tags.

The main idea is to replace the back antenna A_b with a large barrier, *e.g.*, the wall or shelf. The barrier reflects the signals transmitted from A_f to T_{cb}. Then, the signals of T_{cb} will travel back to A_f. The propagation paths of the signals are illustrated in Fig. 12. A_f transmits the signals directly to T_{cf} via the line-of-sight path (1). For

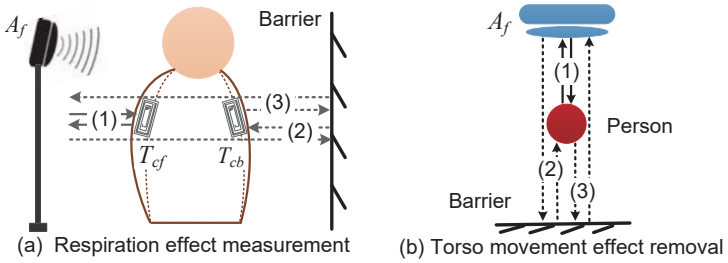

Fig. 12. One-antenna deployment for respiration effect measurement and torso movement effect removal.

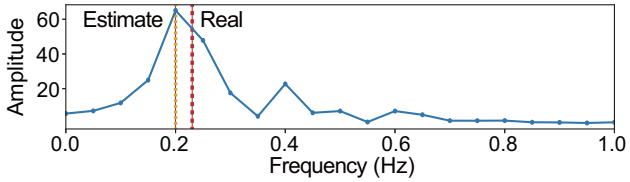

Fig. 13. FFT series of the recovered respiration phase values for respiration rate estimation: the yellow dashed line is the estimated respiration rate and the red dashed line is the real respiration rate.

T_{cb}, the signals first arrive at the barrier, get reflected by it and reach T_{cb} via the multi-path (2). Then, T_{cb} will response to the signals and send out the signals which first reach the barrier, get reflected by it and arrive at A_f via the multi-path (3).

The barrier plays the same role as A_b. For *respiration effect* measurement (Fig. 12(a)), when the person breathes in, the front chest will expand and move forward to A_f, making the length of (1) to decline. Meanwhile, the back chest will move backward to A_f, making the length of (2) and (3) to decrease, too. When the person breathes out, the length of (1), (2) and (3) will all increase. Therefore, the sum of T_{cf} and T_{cb} can help to exaggerate the respiration pattern. For *torso movement effect* removal (Fig. 12(b)), for instance, when the human body moves forward to A_f, the traveling distance of (1) will decrease, while the distance of (2) and (3) will increase inversely. Thus, the summation of the T_{cf} and T_{cb} can also achieve the elimination of the *torso movement effect*. But the concern is that if the barrier is not well positioned, there would not be enough multi-path signals that reach T_{cb} and get back to A_f. Then, the number of the phase values from T_{cb} will not be sufficient to reveal the respiration pattern. We will discuss the influence of the position of the barrier in the evaluation section.

3.5 LRC Estimation

For LRC estimation, intuitively, it can be achieved by dividing f_l over f_r and matching the division result to the nearest LRC ratio in Table 1. However, this method can lead to inaccurate LRC estimation due to the errors in f_r extraction. There can be cases when f_l and f_r are close to each other in practice. The torso *period effect* removed by the Butterworth low-pass filter with f_l as the cutoff frequency has residual effects on the respiration pattern due to the existence of the transition band in the low-pass filter's frequency response. Second, if we perform FFT on the filtered respiration signals within a fixed length of time window , *i.e.*, 20 s, for f_r extraction, the resolution of the frequency domain can be relatively low, *i.e.*, $1/20 = 0.05\ Hz$. This could bring deviations to f_r estimation within the resolution range.

An example of the FFT series for the filtered respiration signals is shown in Fig. 13. We remove the DC component and add a Hamming window on the respiration signals before FFT operation. The f_r is settled as the frequency component with the highest peak, where the first yellow dashed line is located at. The second red

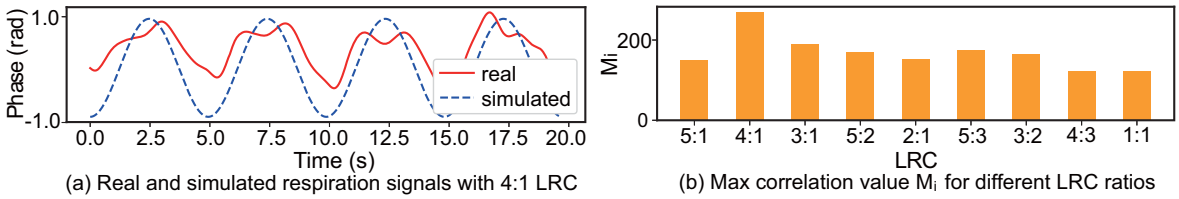

Fig. 14. Correlation-based LRC estimation with the example of the real LRC ratio as 4 : 1

dashed line correspond to the real f_r. There is an 0.03 Hz deviation between the estimated and real respiration rates. The nominator (f_l) is usually larger than the denominator (f_r). Consequently, even a small error in the f_r can lead to wrong LRC estimation. For example, when the real f_l and f_r are 0.6 Hz and 0.24 Hz, respectively, the real LRC ratio should be 5 : 2. However, if there is only 0.03 Hz error less than the real respiration rate, then the LRC would be wrongly estimated as 3 : 1.

To estimate the LRC precisely, we do not extract f_r and calculate LRC directly. Instead, a correlation-based approach is adopted [20]. The insight of this approach is to obtain the most likely LRC based on the prior knowledge of all the possible LRC ratios and limb movement rate f_l. In specific, we leverage the given set of LRC ratios r_i in the LRC list and the estimated f_l, and calculate a set of candidate respiration rates $f_{r_i} = f_l/r_i$. Then, a set of simulated respiration signals are generated with the corresponding f_{r_i} for each of the LRC ratios. The simulated respiration signals are sinusoidal-like time series, represented as follows.

$$s_i(t) = A * \sin(2\pi f_{r_i} t + \phi) \tag{10}$$

The amplitude of the phase series is normalized to $[-1, 1]$. Thus, A is set as 1, and ϕ in Equ. (10) is 0. Then, we calculate the cross-correlation array between the real phase respiration series θ_{real} and each of the simulated respiration signals $s_i(t)$ for different f_{r_i}. Then, we compare the maximum value $M_i = max\{\theta_{real} \cdot s_i(t)\}$ in the correlation array of different LRCs and choose the LRC with the highest M_i as the final ratio. Fig. 14(a) shows an example of the real respiration phase series and the simulated respiration signals with LRC of 4 : 1. The M_i of different LRC ratios are also depicted in Fig. 14(b). The maximum M_i is achieved with the candidate LRC of 4 : 1, which corresponds to the real coupling ratio.

4 EVALUATION

In this section, the experimental setup is first introduced. Then, we will evaluate the accuracy of limb movement rate estimation, respiration rate estimation, and LRC estimation. Next, we will discuss the effects of the distance between the antenna and the person and the effects of the orientation for placing the antenna towards the person on LRC estimation. Meanwhile, we will compare the performance of the two-antenna and one-antenna deployment. Finally, we will show examples of the LRC ratios for persons with different exercise background.

4.1 Experimental Setup

As shown in Fig. 15, the ER-Rhythm system is implemented using COTS RFID devices, including the ImpinJ Speedway R420 RFID reader, Laird E9208 antenna and ImpinJ E41-C tag. The reader works in the $920 - 925$ MHz region, and the reader mode and search mode are set as *AutoSetDence* and *DualTarget*, respectively. The reader is connected to a Dell Inspiron 7460 laptop with $i7 - 7500U$ CPU and 8 GB RAM. The RFID measurements are processed with Python 3.0.

We test the system performance in different environments with five exercise activities, as shown in Fig. 15(b). For cycling and weightlifting, the torso of the exercise could keep relatively stable with small torso movement. For pedaling and rowing, the torso moves along with stepping up-and-down and pulling back-and-forward, in

(a) RFID reader, accelerometer, tag and in-line microphone

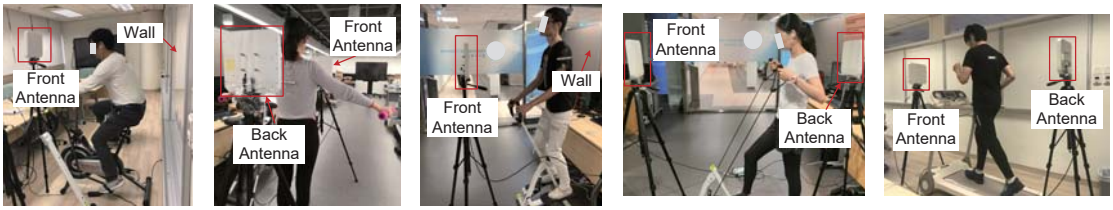

(b) cycling, weightlifting, pedaling, rowing and running under two-antenna or one-antenna deployment

Fig. 15. Illustration of the experiment setup

which the periodic effect plays the main role in affecting the respiration pattern. Running brings the highest torso movement effect because the torso will shake fast and randomly with each stride. All the five activities involve rhythmic and frequent limb movements.

To measure the ground truth of the limb movement rate, a 3-axis accelerator is worn on the leg or arm. To obtain the ground truth of the respiration cycles, we draw from the fact that people perform nasal breathing with louder breathing sound during exercise than in peacetime [4, 30]. Thereby, we ask all the volunteers to breathe via the nose and stick an in-line microphone under the nose to collect the breathing sound during exercise, as shown in Fig. 15(a). To guarantee the effectiveness of breathing sound measurement, we find 5 volunteers and collect their breathing sounds with the microphone. They are guided to breathe 50 times with the commands given by another person beside them. Then, we count the number of peaks in the sound waves, from which all the respiration cycles are correctly detected. In our experiments, 15 volunteers, including 12 males and 3 females, are recruited. They are between 23 and 32 years old ($mean = 26$, $std = 3$), and the between 165 cm and 190 cm tall ($mean = 177\ cm$, $std = 6.5\ cm$). Some of them are regular exercisers with fitness training or sport playing at least twice a week, some rarely exercise. We interview each volunteer about which exercise activities they are interested in and what time they are available for data collection. Then, based on the selected activities, we assign 10 volunteers to each activity. It takes around 10 weeks for all the volunteers to perform the assigned exercise activities during their spare time with 10-20 minutes of training each time.

To evaluate the system performance, three metrics are defined: (1) Mean Absolute Error (MAE) of limb movement rate and respiration rate estimation; MAE is calculated as $\frac{1}{n}\sum_{i=1}^{n}|t_i - e_i|$. t_i and e_i are the true and estimated values, respectively. For each time window, the difference between t_i and e_i is calculated, and the MAE is the average error of all the windows. (2) Percentage of Accurate Windows (PAW) of LRC estimation; For a time period, we divide it into several time windows with fixed length, and the LRC is estimated for each window. Then, we count the number of windows with accurate LRC results over all the windows to get the PAW. For instance, in a 10-min cycling period which involves 30 windows (20s-wide window), the 90% PAW means that 27 windows provide accurate LRC values. We regard the accuracy of LRC is acceptable when PAW is above 90%. (3) Error of LRC estimation; The error of LRC is the difference between the real LRC and the estimated LRC values. For example, the error between the estimated LRC 3 : 1 and the real LRC 2 : 1 is 1, the error between the estimated LRC 5 : 2 and the real LRC 2 : 1 is 0.5. The LRC error is only evaluated for the inaccurately estimated windows. Previous works only evaluate the LRC estimation with the PAW metric [15, 17, 20]. They do not consider the error of LRC estimation. However, we think that the LRC error is also an essential metric to show the LRC estimation

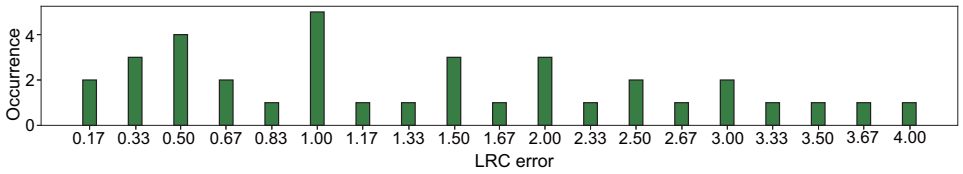

Fig. 16. Statistics of LRC error values

Table 2. Comparison of errors on limb movement and respiration rate estimation with existing works

Limb movement rate	[33]: 1-3 cycles	[39]: 6-8 cycles	Our: 3-5 cycles
Respiration rate	[21]:0.5-1 bpm	[40]: 0.3-0.5 bpm	Our: 0.5-1.5 bpm

performance. [15, 17, 20] mention that the LRC estimation result is acceptable when the estimated LRC is closed to the real one. Therefore, we calculate all the possible LRC errors between every two different LRC values in the LRC List. For instance, the largest error of 4 is the difference between $5:1$ and $1:1$. For repetitive LRC error values, we count their occurrence. For example, the error of 0.17 can be the difference between $3:2$ and $4:3$ or between $5:3$ and $3:2$, so the occurrence is 2. The calculated values of all the possible LRC errors and their occurrence are shown in Table. 16. The median value of all the LRC errors is around 1 (1.17). In addition, the error of 1 has the highest occurrence, which means that it appears more frequently in the wrong LRC estimation windows. Thereby, we empirically regard that if the LRC error is below 1, the estimated LRC is closed to the real one, and vice versa. Furthermore, as mentioned in Section 2.1, exercisers will transit between DC and SC, and SC also reflects the exercise rhythm. So, if the LRC error is the difference between DC and SC, the LRC estimation result is still referential. Since integer LRCs are more commonly seen in exercisers, DC and SC are more likely to be integer LRCs. Hence, the difference between DC and SC is usually 1. Based on the above statistics of LRC errors, we empirically set the acceptable LRC error range to be the values below 1.

4.2 Limb Movement Rate and Respiration Rate Estimation

Here, the evaluation is done under the two-antenna deployment. The distance between the person and antenna is 1 m, and the antenna is put on a tripod with $1.5 - 1.8$ m high based on the person's height.

4.2.1 Limb Movement Rate Estimation. The average MAE of limb movement rate estimation is 0.008 Hz. We evaluate the performance of limb movement rate estimation for different exercise activities. For running, pedaling and cycling, the tag on the leg is used for extracting the limb movement rate. For weightlifting and rowing, the tag on the arm is used. We compare the estimation accuracy of attaching the tags on different limb parts. For the arm, the tag can be put on the upper or lower arm. For the leg, the tag can be put on the thigh or the knee. The results are shown in Figure 17(a). The MAEs are all below 0.015 Hz, indicating the estimated rate is quite close to the ground truth. In addition, the MAEs of putting the tags on the lower arm and on the knee are smaller than that on the upper arm and thigh, and the average MAE is around 0.008 Hz. This is because the tags on the lower arm and knee experience longer distance change, so the movement pattern is more obvious. We also compare the accuracy of limb movement rate estimation with [33] and [39]. [33] uses the smartwatch to estimate weightlifting cycles, and [39] uses WiFi signals to estimate running steps. Since they use the metric with the error of cycles during a period, we convert the MAE of limb movement rate in the unit of Hz to the number of wrong detected cycles of limb movements. The results are shown in Table 2. The comparison results show that the accuracy of limb movement rate estimation is better than that in [39], while worse than that in [33]. According to the survey in [33], the average error of $3 - 5$ cycles is tolerable for the users.

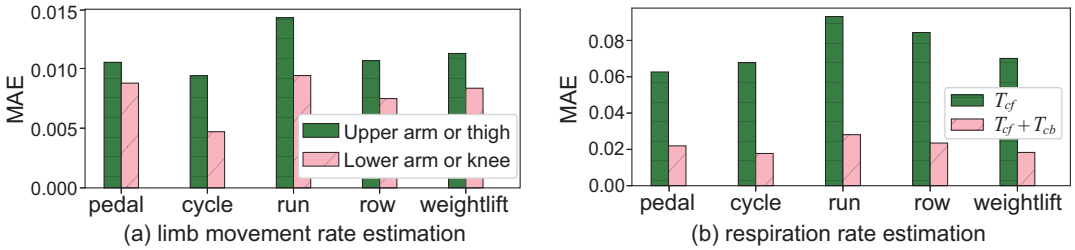

Fig. 17. MAEs of estimating limb movement rate and respiration rate.

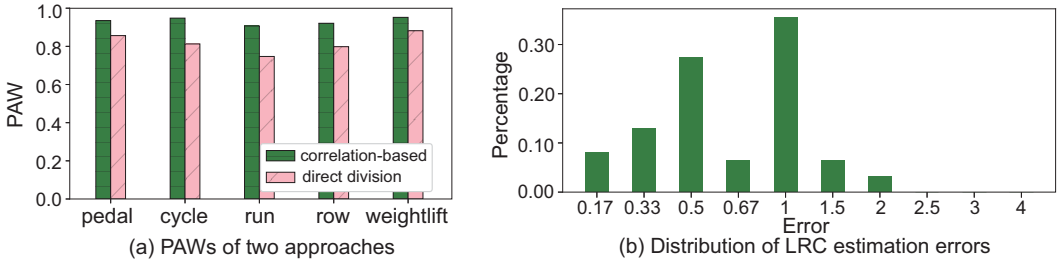

Fig. 18. PAWs and errors of LRC estimation

4.2.2 Respiration Rate Estimation. The average MAE of respiration estimation is about 0.0225 Hz. Next, we perform experiments to evaluate the effectiveness of our method for extracting respiration rhythm during exercise and compare with the performance of only using T_{cf}'s phase profile. Although we do not calculate the LRC by estimating the respiration rate directly from the summation phase profile, the accuracy of respiration rate estimation is discussed here for comparison. We perform FFT on the summation phase profile of T_{cf} and T_{cb} after chest movement measurement and torso movement effect removal and on the phase profile of T_{cf} after signal pre-processing and low-pass filtering. As depicted in Fig. 17(b), using only the phase values collected from T_{cf}, the average MAE can be around 0.071 Hz, which is equal to around 4.3 breath per minute. While, with the summation phase values (T_{cf} and T_{cb}), the average MAE is about 0.0225 Hz, corresponding to 1.35 breath per minute. The MAE of respiration rate estimation is reduced by two-thirds. We compare the MAE of respiration rate estimation with [21] and [40], as shown in Table 2. For respiration rate estimation, the MAE of our work is a little larger than that of [21] and [40]. Because the assumption in [21, 40] is that the target person is quasi-static, while our system is for the exercise scenario, where the movements make the respiration pattern noisier. Nevertheless, we do not directly use the respiration rate to estimate the LRC. Instead, the correlation-based approach is applied to improve the accuracy of LRC estimation.

4.3 LRC Estimation

The LRC estimation is evaluated with respect to different approaches, distances, and orientations under both two-antenna and one-antenna deployment.

4.3.1 Comparison of different LRC estimation approaches. The correlation-based approach can achieve higher accuracy on LRC estimation. The performance of LRC estimation with different approaches is evaluated under the two-antenna deployment with 1 m distance between the antenna and target human. We first compare the PAW results of directly dividing the limb movement rate over the respiration rate with those of our proposed correlation-based approach, as shown in Fig. 18(a). The average PAW of the direct division approach is around

Table 3. PAW of LRC estimation for different persons and different exercise activities

Person	1	2	3	4	5	6	7	8	9	10
PAW - pedal	93.8%	94%	94.4%	93.4%	93.1%	92.8%	94.7%	93.6%	93%	92.2%
Main LRC - pedal	2:1	3:1	3:1	2:1	4:1	4:1	2:1	3:1	2:1	3:1
PAW -cycle	94.4%	95.2%	96%	94.7%	94.4%	93.5%	95%	94.8%	95.2%	94.8%
Main LRC - cycle	3:1	3:1	2:1	4:1	3:1	4:1	3:1	3:1	2:1	3:1
PAW -run	93%	91.1%	92.8%	89.4%	90.8%	92%	90.4%	90%	89%	89.2%
Main LRC - run	2:1	2:1	3:1	4:1	2:1	3:1	2:1	2:1	4:1	2:1
PAW -row	93.5%	94.1%	92%	91.5%	91.7%	91.2%	92%	92.3%	91.5%	91.2%
Main LRC - row	2:1	3:1	3:2	3:1	5:2	2:1	2:1	3:2	3:1	4:3
PAW - lift	96%	95.2%	94.1%	95%	93.8%	95.5%	96%	95.8%	95%	95.6%
Main LRC - lift	3:2	2:1	2:1	3:2	3:2	5:2	2:1	3:2	2:1	2:1

81%, which is lower than the average PAW of the correlation-based approach (92%). The main reason is that errors in respiration rate estimation can lead to large deviation in LRC estimation. While the correlation-based approach narrows the range of possible results by using the potential LRC ratios. We further show the detailed PAW results and main LRC ratios for different activities and each of the 10 persons in Table 3. The main LRC is the ratio that appears most frequently for the person performing the specific exercise activity. Generally, the PAW results for the running (90.7%) and rowing (92.1%) activities are smaller than those of pedaling (93.5%), cycling (94.8%) and lifting (95.2%). This is because that larger torso movement is involved during running and rowing, which incurs more noises to the respiration pattern extraction. Compared with existing smartphone-based systems [17, 20], whose PAW is around $91-91\%$, our approach achieves the comparable results.

We also show the distribution of the errors between the real and the estimated LRCs for the correlation-based approach in Fig. 18(b). There are 19 possible error values among all the LRC ratios, while in our experiments, there are 10 error values that appear. The average error of all the samples is 0.74. The frequent error values are 0.5 and 1, and there is no error larger than 2. Thus, the errors in LRC estimation of our system are within a small range. Besides, we find out the errors of which the estimated LRC is the neighbor of the real LRC, and the neighbor errors account for 72% of all the errors. This indicates that, even though some errors appear, the estimation LRC ratio is not far from the real one.

4.3.2 Distance. The PAWs of LRC estimation are above 85% *when the distance between the antenna and target person is within* 2.5 *m for the two-antenna deployment, and the PAWs are above* 85% *for the one-antenna deployment when the distance is within* 1.5 *m. The average errors of LRC are below* 1 *within* 2.5 *m for the two-antenna deployment and within* 1 *m for the one-antenna deployment.* First, we investigate the effects of the distance between the front/back antenna and target person on LRC estimation for the two-antenna deployment. Here, the target person faces the antenna straight. There are furniture and other objects in the environment. The PAWs are shown in Fig. 19(a). Within 2.5 *m*, the PAWs are above 85%. For longer distance, the performance degrades gradually. For distance longer than 4 *m*, there are cases that the RFID reader fails to read enough phase values of the tags (no signal measurements or the number of the measurements is below 10 per second), so there is no PAW result. The average errors of LRC estimation for the two-antenna deployment are given in Table 4. The errors are lower than 1 when the distance is within 2.5 *m*, and keep increasing with longer distance. Longer distance also brings a problem that there can be other persons moving in the area between the target person and the antenna or the objects in this area block the signals. We did experiments when the distance between the antenna and person is 2.5 *m*, and one person is asked to walk randomly in the LOS area between the antenna and the target person. The PAW of LRC estimation drops to 67%. This shows that the system performance can be affected by the movements intervening the LOS signals. Thereby, the antennas should be put closed to the target person, *e.g.*, $1-1.5$ *m*, to avoid objects' blockage and people's movements.

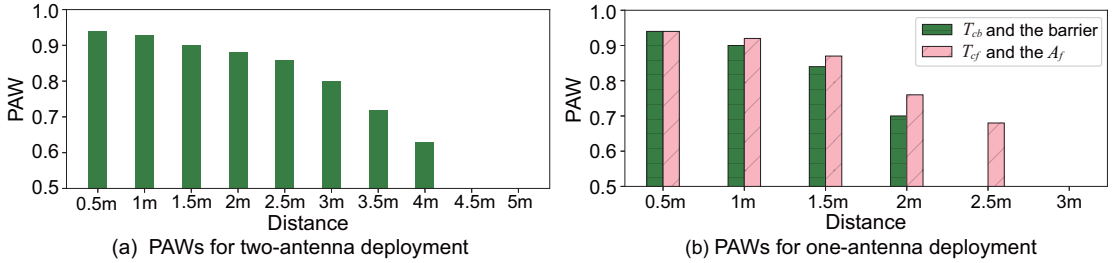

Fig. 19. Effects of distance on LRC estimation

Table 4. Average errors of LRC estimation for different distances

Distance(m)	0.5	1	1.5	2	2.5	3	3.5	4
LRC error of two-antenna deployment	0.71	0.74	0.79	0.86	0.95	1.13	1.38	1.84

3*LRC error of one-antenna deployment	Distance(m)	0.5	1	1.5	2	2.5
	T_{cb} and barrier	0.85	0.91	1.12	1.64	/
	T_{cf} and A_f	0.82	0.88	0.95	1.43	1.87

Next, we discuss the effects of the distance between T_{cb} and the barrier and that between T_{cf} and A_f on LRC estimation for the one-antenna deployment. Here, we use the indoor wall and clapboard as large barriers, as shown in Fig. 15(b). First, the distance between T_{cf} and A_f is fixed to 1 m, and we test the effects of the distance between the T_{cb} and the barrier on LRC estimation. Then, we fixed the distance between T_{cb} and the barrier to 1 m and change the distance between T_{cf} and A_f reversely. As shown in Fig. 19(b), when the distance between T_{cf} and A_f, and that between T_{cb} and the barrier are within 1.5 m, the values of PAW are above 80%. With the distance becoming longer, the accuracy could decrease. The average errors of LRC for the one-antenna deployment are also shown in Table 4. For the same distance between the T_{cb} and the barrier and that between T_{cf} and A_f, the error of the former setting is larger than that of the latter one. In addition, we find that the performance is more sensitive to the distance between the T_{cb} and the barrier: there are not enough signal measurements collected when the distance is above 2 m. While the upper limit of the distance between the T_{cb} and the antenna can reach 2.5 m to receive signals. This is due to the reason that the RFID signals, reflected by the barrier and back to the receiver, lose more power in this process. The number and the power of the received signals of T_{cb} would be less than that of the T_{cf}. Thus, for the one-antenna deployment, it requires the distance among the person, the antenna and the barrier to be shorter.

4.3.3 Orientation. The PAWs of LRC estimation are above 85% *when the orientation is within* 20° *for the two-antenna deployment, and the PAWs are above* 80% *when the orientation is within* 20° *for the one-antenna deployment. The average errors of LRC are below* 1.5 *within* 30° *for the two-antenna deployment and within* 20° *for the one-antenna deployment.* The orientation of the target person towards the antenna, α, is defined as depicted in Fig. 20, and we discuss the effects of the orientation on LRC estimation. Here, the distance between the antenna/barrier and the target person is fixed to around 1 m. For the two-antenna deployment, as shown in Fig. 21, when α is within 20°, the PAWs are above 85%. However, when α keeps growing, the PAW becomes worse, even below 60% for α of 50°. When α is 60°, there are not enough signal measurements received by the RFID readers because the antenna is directional. The average errors of LRC for the two-antenna deployment are shown in Table 5. The average errors exceed 1.5 when α is above 30°. The reason why the LRC estimation accuracy drops so quickly after 30° is two-fold. First, there would be fewer signals collected by the reader with a larger α as the directional antenna has a limit ellipsoidal reading zone. Second, when α increases, the chest displacement will have smaller effects on the

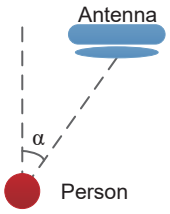

Fig. 20. Illustration of the orientation of the person towards the antenna.

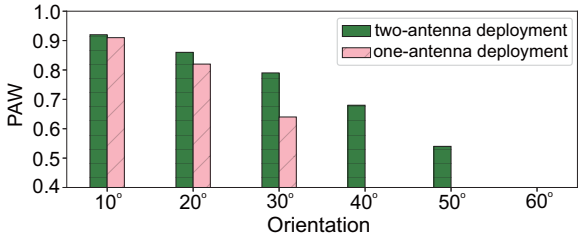

Fig. 21. PAWs of the LRC estimation with different orientation angles for the two-antenna and one-antenna deployment.

Table 5. Average errors of LRC estimation for different orientation angles

α	10°	20°	30°	40°	50°
LRC error of two-antenna deployment	0.81	0.92	1.26	1.75	2.17
LRC error of one-antenna deployment	0.85	1.08	1.63	2.04	/

Table 6. PAWs and average errors for the multi-person scenario

No.-Activities	2-[pedal, cycle]	2-[pedal, weight lift]	2-[cycle, run]	3-[pedal, cycle, run]
PAW	[92%, 89%]	[91%,88%]	[88%, 90%]	[90%, 86%, 89%]
Error	[0.81, 0.86]	[0.83, 0.90]	[0.93, 0.85]	[0.94, 1.05, 0.91]

change of the propagation path for the signals. Thereby, the respiration pattern could be less clear which could result in lower PAW for LRC estimation.

The effects of α on the LRC estimation for the one-antenna deployment follow the similar trend of the two-antenna deployment. The PAWs decrease with the increment of α, and the reader cannot receive enough signals, especially for T_{cb} when α is and above 40°. As illustrated in Table 5, the one-antenna deployment reports more errors compared with those of the two-antenna deployment. The average error exceeds 1 when α is 20°. The orientation has more dramatic influence on LRC estimation since the PAW drops down faster and the error becomes larger. The upper limit of α (40°) is smaller than that of the two-antenna deployment (50°). This means that for the one-antenna deployment, the antenna should be better deployed with smaller α. In practice, the antennas can be displaced down from the ceiling and put right in front of (and behind for two-antenna deployment) the exercise equipment. This not only helps to achieve better estimation results but also benefits the monitoring of multiple persons so that the signals of multiple persons could interfere less with each other.

4.3.4 Multi-person scenario. The PAWs of the multi-person scenario are above 86% *and the average errors are below* 1.05. The above experiments are done with a single person. In practice, there can be multiple persons doing exercise together. Like in the gym, multiple persons could run on the treadmill. Besides, different kinds of exercise equipment can be put along with each other. Thus, we need to evaluate the LRC estimation performance with multiple persons and with different combinations of exercise activities. As we discussed in subsection 4.3.2, the surrounding movements could affect the target persons' signals, especially when the movements influence the LOS signals. So, for the multi-person scenario, each person has the unique RFID tags attached on their bodies, and multiple pairs of antennas are put in front of and behind each of them, respectively. The persons are located horizontally without burying others' signals, then there could be only the minor multi-path effects brought by the neighbor persons.

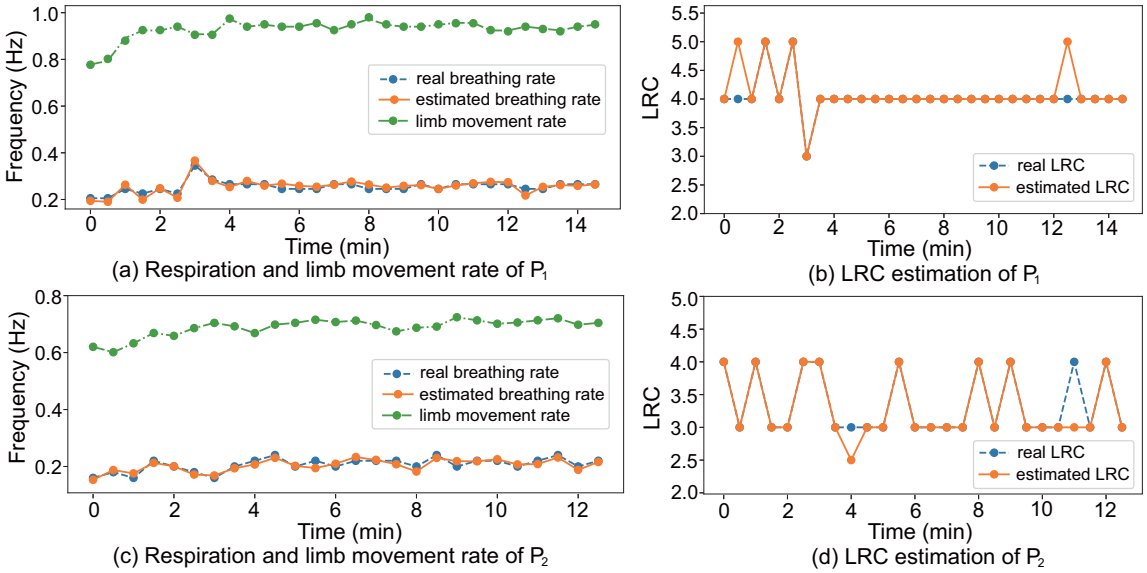

Fig. 22. Illustration of respiration rate and LRC estimation over time

To evaluate the performance of multi-person LRC estimation, two persons are first asked to perform the following set of the exercise, (pedaling, cycling), (pedaling, lifting) and (cycling, running), respectively. In addition, three persons perform the pedaling, cycling and lifting at the same time. The distance between each two of the multiple persons is around $1 - 1.5$ m. The results of the PAW and average error are shown in Table 6. For two persons, the PAW is approximately around 90%, and the average error is around 0.85. For three persons, the person in the middle has lower accuracy (PAW about 86%, error about 0.97) due to the reason that the two persons around both bring multi-path effects to the middle person.

4.4 LRC Illustration over Time

In this subsection, we show the detailed LRC ratios for two selected volunteers during exercise in Fig. 22. The first person (P_1) in Fig. 22(a)-(b) is a football lover with fitness training around three times a week. While the second person (P_2) in Fig. 22(c)-(d) does not exercise regularly, and in the experimental period, he did not go to the gym or exercise outdoor specifically except for the experimental exercise. For P_1, we show the real and estimated LRC ratios of each time window discretely for the running activity. In Fig. 22(b), there are a few fluctuations of the LRC ratios in the beginning, and then it becomes stable as $4:1$. There are two wrong LRC estimation samples along the 15 min period. The estimated and real limb movement rate and respiration rate are also depicted in Fig. 22(a). There is a gradual increase in both the limb movement rate and respiration rate during the first $4 - 5$ minutes. For P_2, the limb movement rate, respiration rate are and the LRC ratios, are also shown for the running activity in Fig. 22(c)-(d).

Comparing the exercise and respiration information of P_1 with P_2, P_1 has higher limb movement rate and LRC ratio than P_2. This is mainly because that P_2 goes for fitness training and sports less than P_1, so P_1 tend to run slower than P_2. For P_1, the respiration rate is more stable than that of P_2. Meanwhile, the LRC ratios of P_2 after 4 minutes illustrate more fluctuations than P_1. The above results could indicate that people who exercise frequently could foster better cardio-pulmonary function. Therefore, they can achieve more stable coordination between the exercise and respiration rhythm than those who are not regular exercisers. We also inquiry P_1 about his way of

breathing during exercise. The answer is that P_1 keeps the habit of fixing his respiration rhythm along with the leg movement cycle during running, which he learned from professionals that this could help to strengthen the exercise performance.

5 RELATED WORK

We first introduce the existing systems for exercising-only monitoring and respiration-only monitoring, respectively. Next, we discuss the related works for exercise and respiration rhythm monitoring.

5.1 Exercise-only Monitoring

There are many wearable devices and sensors for monitoring exercise activities. The inertial sensors, *e.g.*, the accelerometer and gyroscope in wearable devices are widely used to measure the exercise movement, for example, the stride frequency and running speed. They can also provide fine-grained information to assess the behavior during exercise [18, 33]. In addition, current smartwatches can monitor the heart rate based on the photoplethysmography[2]. However, except for the heart rate, the respiration rate is also one of the important vital signs. Cameras can also be used for exercise monitoring [23], however, people in the public gym would not like to be captured by the cameras due to the privacy concerns.

Apart from the wearable sensors, there are device-free approaches for exercise monitoring using RF signals. People only need to attach RFID tags or even do not need to wear any sensors on their bodies for being monitored. In [14], it builds a platform to monitor free-weight exercises, including free-weight activity recognition and performance assessment with RFID. [39] estimates the running steps for multiple persons using WiFi signals. [19] realizes indoor workout assessment with WiFi signals. However, the above works only capture the exercise limb movement information but without the respiration state.

5.2 Respiration-only Monitoring

Respiration monitoring systems involve two categories, which are device-based and device-free systems. Device-based approaches rely on on-body sensors, *e.g.*, belt on the chest and oximeter on the finger [8]. They can provide precise monitoring of the respiration state, however, the sensors tightly worn on the body could make people feel uncomfortable, especially during sleeping. Therefore, the device-free respiration monitoring based on wireless signals is proposed in which people do not need to wear any sensors on the body. The underlying principle of using wireless signals for respiration monitoring is that the chest movement can affect the propagation of the wireless signals periodically.

Recently, RF signals, *e.g.*, WiFi [25, 37, 38], Doppler radar [29], FMCW radar [9, 36], and acoustic signals [35] are leveraged to monitor the respiration rate in a non-intrusive way. RFID is also used for respiration monitoring by attaching tags on the chest [21]. However, one limitation of the above works is that they can only monitor the respiration accurately when the person is in a quasi-static state, like sleeping or sitting still. This is mainly because when the person moves, the large body movement could overwhelm the tiny chest movement during respiration. While for some exercise activities, the body movement could be more fierce, making the extraction of respiration pattern suffer from greater noises.

5.3 Exercise and Respiration Rhythm Monitoring

The CPET system provides a clinical tool for monitoring the respiratory and cardiac functions during exercise [1]. By measuring the physiological signals, including the breathing volume, heart rate, and ECG, it enables an integral view of the exercise capacity. However, for daily exercise monitoring, it cannot be widely applied for the following two reasons. First, the CPET system involves many sensors, *e.g.*, the facemask, ECG electrodes, and

tonometer, which are inconvenient to wear during regular exercise. Second, a single CPET test can cost up to around $2,000, which people would not like to afford for common use.

To ease the above requirements, some systems, that measure the breathing sound with the headset connected to the smartphone [15, 16, 20] during running, are proposed. The breathing sound generated via the air flow from the nose [24] is used to reflect the respiration cycle, and the inertial sensors in the smartphone on the arm measure the stride frequency. The LRC ratio is then estimated by combining the respiration and stride movement information. They provide a cost-effective solution for monitoring the exercise and respiration rhythm. However, people still need to attach the specialized headset close to the nose and carry the smartphone along with them while doing exercise. Furthermore, the smartphone on the arm cannot capture the leg movement pattern, restricting the application scenarios.

Different from the existing works, our work presents a novel approach for coupling the exercise and respiration rhythm using COTS RFID. The lightweight RFID tags are attached on the body, making people get rid of the bulky sensors. The RFID devices can be deployed in different indoor environments for public use, so that exercisers do not need to buy their personal devices and save the cost with the inexpensive RFID tags for monitoring LRC. In contrast with the previous works that either only monitor the exercise activities or the mere respiration state, our system can extract the rhythm of the exercise movement and respiration simultaneously and accurately estimates the LRC ratio.

6 LIMITATIONS AND FUTURE WORK

ER-Rhythm realizes the coupling of exercise and respiration rhythm in a low-cost, lightweight and accurate way. However, in the current system, we mainly target on the in-place rhythmic exercise activities, which do not incur large position change in exercise. While there are some exercise activities, like yoga and aerobic dancing, in which people may move around more obviously, making the torso movement effect more complicated. In the future, we will try to broaden the application of our system for more kinds of exercise activities. In addition, heart rate is also an important physiological indicator during exercise apart from the respiration state. Therefore, we will also investigate the capability of the RFID signals to measure the heart rate while exercising, which could be a quite challenging task since the heartbeat effect is even smaller than the respiration effect.

7 CONCLUSION

In this paper, we propose ER-Rhythm to simultaneously measure the exercise and respiration rhythm and estimate the LRC using the lightweight and COTS RFID. The RFID tags are attached on the limbs and chest to capture the exercise limb movement and respiration pattern. The limb movement rhythm is estimated by analyzing the signals of the tags on limbs via peak detection. However, the minute respiration activity is overwhelmed by the large torso movement during exercise. To obtain clear respiration pattern, we employ the respiration mechanism to measure the chest movement while breathing by combining the signals of the pair of tags on the front and back chest. Meanwhile, the torso movement effects are eliminated by fusing the information of multiple tags. We can also reduce the number of antennas for interrogating the multiple tags by employing the multi-path effects of the RF signals. Finally, the LRC is estimated with a correlation-based approach to determine the coupling between the exercise locomotion and respiration. Experimental results show that we can achieve an average $0.0225\ Hz$ MAE on respiration rate estimation during exercise, and the LRC ratio can be correctly estimated for $92\% - 95\%$ of the time.

ACKNOWLEDGMENTS

The work is supported by the National Key R&D Program of China (No. 2018YFB1004801) and the Shenzhen Basic Research Funding Scheme (No. JCYJ20170818104222072).

REFERENCES

[1] 2009. Cardio pulmonary exercise test: CPET. https://www.ucl.ac.uk/anaesthesia/research/CPET.

[2] 2015. How do smart watches measure the heart beat on the wrist? https://www.quora.com/How-do-Smart-Watches-measure-the-heart-beat-on-the-wris.

[3] 2017. 10 scary side effects of over exercising. https://www.femina.in/wellness/fitness.

[4] 2017. Nasal breathing for exercise. https://www.ceenta.com/news-blog/follow-your-nose-to-better-exercise-habits.

[5] 2018. Stride frequency in running. https://posemethod.com/stride-frequency.

[6] 2019. Cadence(cycling). https://en.wikipedia.org/wiki/Cadence (cycling).

[7] 2019. Medtronic Bioharness. https://www.zephyranywhere.com.

[8] 2019. Pulse oximetry. https://en.wikipedia.org/wiki/Pulse oximetry.

[9] Fadel Adib, Hongzi Mao, Zachary Kabelac, Dina Katabi, and Robert C Miller. 2015. Smart homes that monitor breathing and heart rate. In *Proceedings of the ACM conference on human factors in computing systems (CHI)*.

[10] Khaled Albouaini, Mohaned Egred, Albert Alahmar, and David Justin Wright. 2007. Cardiopulmonary exercise testing and its application. *Postgraduate medical journal* 83, 985 (2007), 675–682.

[11] RR Bechbache and J Duffin. 1977. The entrainment of breathing frequency by exercise rhythm. *The Journal of physiology* 272, 3 (1977), 553–561.

[12] Paolo Bernasconi and Jana Kohl. 1993. Analysis of co-ordination between breathing and exercise rhythms in man. *The Journal of physiology* 471, 1 (1993), 693–706.

[13] Dennis M Bramble and David R Carrier. 1983. Running and breathing in mammals. *Science* 219, 4582 (1983), 251–256.

[14] Han Ding, Longfei Shangguan, Zheng Yang, Jinsong Han, Zimu Zhou, Panlong Yang, Wei Xi, and Jizhong Zhao. 2015. Femo: A platform for free-weight exercise monitoring with RFIDs. In *Proceedings of the 2015 ACM Conference on Embedded Networked Sensor Systems (Sensys)*.

[15] Fei Gu, Jianwei Niu, Sajal K Das, and Zhenxue He. 2016. An efficient method of detecting breathing frequency while running. In *Proceedings of the 2016 IEEE International Conference on Smart Computing (SMARTCOMP)*.

[16] Fei Gu, Jianwei Niu, Sajal K Das, and Zhenxue He. 2018. Runnerpal: A runner monitoring and advisory system based on smart devices. *IEEE Transactions on Services Computing* 11, 2 (2018), 262–276.

[17] Fei Gu, Jianwei Niu, Sajal K Das, Zhenxue He, and Xin Jin. 2017. Detecting breathing frequency and maintaining a proper running rhythm. *Pervasive and Mobile Computing* 42 (2017), 498–512.

[18] Xiaonan Guo, Jian Liu, and Yingying Chen. 2017. FitCoach: Virtual fitness coach empowered by wearable mobile devices. In *Proceedings of the 2017 IEEE Conference on Computer Communications (INFOCOM)*.

[19] Xiaonan Guo, Jian Liu, Cong Shi, Hongbo Liu, Yingying Chen, and Mooi Choo Chuah. 2018. Device-free Personalized Fitness Assistant Using WiFi. In *Proceedings of the 2018 ACM on Interactive, Mobile, Wearable and Ubiquitous Technologies*.

[20] Tian Hao, Guoliang Xing, and Gang Zhou. 2015. RunBuddy: a smartphone system for running rhythm monitoring. In *Proceedings of the 2015 ACM International Joint Conference on Pervasive and Ubiquitous Computing (Ubicomp)*.

[21] Yuxiao Hou, Yanwen Wang, and Yuanqing Zheng. 2017. Tagbreathe: Monitor breathing with commodity RFID systems. In *Proceedings of the 2017 IEEE International Conference on Distributed Computing Systems (ICDCS)*.

[22] JA Scott Kelso et al. 1995. The self-organization of brain and behavior. *Lecture Notes in Complex Systems, Santa Fe, NM* (1995).

[23] Rushil Khurana, Karan Ahuja, Zac Yu, Jennifer Mankoff, Chris Harrison, and Mayank Goel. 2018. GymCam: Detecting, Recognizing and Tracking Simultaneous Exercises in Unconstrained Scenes. In *Proceedings of the 2018 ACM on Interactive, Mobile, Wearable and Ubiquitous Technologies*.

[24] Eric C Larson, Mayank Goel, Gaetano Boriello, Sonya Heltshe, Margaret Rosenfeld, and Shwetak N Patel. 2012. SpiroSmart: using a microphone to measure lung function on a mobile phone. In *Proceedings of the 2012 ACM Conference on Ubiquitous Computing (Ubicomp)*.

[25] Jian Liu, Yan Wang, Yingying Chen, Jie Yang, Xu Chen, and Jerry Cheng. 2015. Tracking vital signs during sleep leveraging off-the-shelf WiFi. In *Proceedings of the 2015 ACM International Symposium on Mobile Ad Hoc Networking and Computing (MobiHoc)*.

[26] Xuefeng Liu, Jiannong Cao, Shaojie Tang, and Jiaqi Wen. 2014. Wi-Sleep: Contactless sleep monitoring via WiFi signals. In *Proceedings of the 2014 IEEE Real-Time Systems Symposium (RTSS)*.

[27] William J McDermott, Richard EA Van Emmerik, and Joseph Hamill. 2003. Running training and adaptive strategies of locomotor-respiratory coordination. *European journal of applied physiology* 89, 5 (2003), 435–444.

[28] L Persegol, M Jordan, and D Viala. 1991. Evidence for the entrainment of breathing by locomotor pattern in human. *Journal de physiologie* 85, 1 (1991), 38–43.

[29] Tauhidur Rahman, Alexander T Adams, Ruth Vinisha Ravichandran, Mi Zhang, Shwetak N Patel, Julie A Kientz, and Tanzeem Choudhury. 2015. Dopplesleep: A contactless unobtrusive sleep sensing system using short-range doppler radar. In *Proceedings of ACM International Joint Conference on Pervasive and Ubiquitous Computing (Ubicomp)*.

[30] Christine Recinto, Theodore Efthemeou, P Tony Boffelli, and James W Navalta. 2017. Effects of Nasal or Oral Breathing on Anaerobic Power Output and Metabolic Responses. *International journal of exercise science* 10, 4 (2017), 506.
[31] G Robertson, G Caldwell, J Hamill, G Kamen, and S Whittlesey. 2013. Research Methods in Biomechanics, 2E. Human Kinetics.
[32] Ghufran Shafiq and Kalyana C Veluvolu. 2014. Surface chest motion decomposition for cardiovascular monitoring. *Scientific reports* 4 (2014), 5093.
[33] Chenguang Shen, Bo-Jhang Ho, and Mani Srivastava. 2018. Milift: Efficient smartwatch-based workout tracking using automatic segmentation. *IEEE Transactions on Mobile Computing* 17, 7 (2018), 1609–1622.
[34] Abigail SL Stickford and Jonathon L Stickford. 2014. Ventilation and Locomotion in Humans: Mechanisms, Implications, and Perturbations to the Coupling of These Two Rhythms. *Springer Science Reviews* 2, 1-2 (2014), 95–118.
[35] Tianben Wang, Daqing Zhang, Yuanqing Zheng, Tao Gu, Xingshe Zhou, and Bernadette Dorizzi. 2018. C-FMCW based contactless respiration detection using acoustic signal. In *Proceedings of the 2018 ACM on Interactive, Mobile, Wearable and Ubiquitous Technologies*.
[36] Shichao Yue, Hao He, Hao Wang, Hariharan Rahul, and Dina Katabi. 2018. Extracting multi-person respiration from entangled RF signals. *Proceedings of the ACM on Interactive, Mobile, Wearable and Ubiquitous Technologies*.
[37] Youwei Zeng, Dan Wu, Ruiyang Gao, Tao Gu, and Daqing Zhang. 2018. FullBreathe: Full Human Respiration Detection Exploiting Complementarity of CSI Phase and Amplitude of WiFi Signals. In *Proceedings of the 2018 ACM on Interactive, Mobile, Wearable and Ubiquitous Technologies*.
[38] Fusang Zhang, Daqing Zhang, Jie Xiong, Hao Wang, Kai Niu, Beihong Jin, and Yuxiang Wang. 2018. From fresnel diffraction model to fine-grained human respiration sensing with commodity Wi-Fi devices. In *Proceedings of the 2018 ACM on Interactive, Mobile, Wearable and Ubiquitous Technologies*.
[39] Lei Zhang, Meiguang Liu, Liangfu Lu, and Liangyi Gong. 2018. Wi-Run: Multi-Runner Step Estimation Using Commodity Wi-Fi. In *Proceedings of the 2018 Annual IEEE International Conference on Sensing, Communication, and Networking (SECON)*.
[40] Run Zhao, Dong Wang, Qian Zhang, Haonan Chen, and Anna Huang. 2018. CRH: A Contactless Respiration and Heartbeat Monitoring System with COTS RFID Tags. In *Proceedings of the 15th Annual IEEE International Conference on Sensing, Communication, and Networking (SECON)*.